Mittelholz, A., Johnson, C. L., Morschhauser, A. (2018): A New Magnetic Field Activity Proxy for Mars From MAVEN Data. - *Geophysical Research Letters*, *45*, 12, pp. 5899—5907.

DOI: http://doi.org/10.1029/2018GL078425

AGU100 ADVANCING EARTH AND SPACE SCIENCE

Geophysical Research Letters

RESEARCH LETTER
10.1029/2018GL078425

Key Points:
- MAVEN IMF magnitude measurements can be used as a magnetic proxy at Mars
- Magnetically quiet and noisy data can be separated
- We demonstrate an application of the proxy by selecting quiet data for crustal field modeling

Correspondence to:
A. Mittelholz,
amittelh@eoas.ubc.ca

Citation:
Mittelholz, A., Johnson, C. L., & Morschhauser, A. (2018). A new magnetic field activity proxy for Mars from MAVEN data. *Geophysical Research Letters*, *45*, 5899–5907. https://doi.org/10.1029/2018GL078425

Received 19 APR 2018
Accepted 31 MAY 2018
Accepted article online 11 JUN 2018
Published online 26 JUN 2018

A New Magnetic Field Activity Proxy for Mars From MAVEN Data

A. Mittelholz[1], C. L. Johnson[1,2], and A. Morschhauser[3]

[1]Department of Earth, Ocean and Atmospheric Sciences, The University of British Columbia, Vancouver, British Columbia, Canada, [2]Planetary Science Institute, Tucson, AZ, USA, [3]GFZ German Research Centre for Geosciences, Potsdam, Germany

Abstract The identification of magnetically quiet or noisy observations is important for data selection in a wide range of studies, including crustal field modeling and investigations of the ionosphere. However this remains a challenge when studying the magnetic field of Mars, as no continuous magnetic activity index is available. Such indices are widely used for studies of Earth's magnetic field, and they are largely based on data from ground observatories. We suggest a martian magnetic activity proxy based on satellite data, from the Mars Atmosphere and Volatile EvolutioN spacecraft (MAVEN). MAVEN has been in orbit since November 2014, providing measurements of the magnetic field that extend those from the Mars Global Surveyor mission. The proxy uses the magnitude of the interplanetary magnetic field upstream of the bow shock and is motivated by the correlation of the interplanetary magnetic field amplitude with the nightside magnetic field at 150- to 600-km altitude, measured on the same MAVEN orbit. We demonstrate the utility of the proxy, by producing a model of the surface crustal field in a previously mapped low-amplitude region in the vicinity of the InSight landing site. The proposed proxy successfully separates quiet and noisy data and will facilitate MAVEN data selection for higher-resolution crustal field models. Other applications include data selection for magnetic sounding studies using the InSight magnetometer, or studies of the ionosphere. The deployment of a ground-based magnetometer by InSight will also allow the refinement of the proxy, using simultaneous satellite and surface magnetic field measurements.

Plain Language Summary The ability to distinguish between magnetically quiet and noisy data measured at or above the surface of a planet is important for a wide range of studies. For example, high fidelity models of the crustal magnetic field require data that contain minimal signals from other sources—i.e., that are quiet. At Earth, such data selection uses estimates of magnetic activity (so-called activity indices or proxies) derived from ground-based magnetic observatories. We propose a proxy for magnetic field activity at Mars, where no ground-based measurements are yet available, that uses magnetic data from the MAVEN spacecraft. The proxy is based on the correlation of the magnetic field measured in the solar wind and that measured closer to the planet, out of the solar wind, on the nightside. We show an application of the proxy by developing an updated crustal field model in the vicinity of the InSight landing site. The InSight mission will provide the first surface magnetic field measurements at Mars, and the opportunity to refine the proposed proxy.

1. Introduction

The Mars Global Surveyor (MGS) spacecraft operated from 1997 to 2006 and provided a wealth of information on the martian magnetic field environment including the unexpected discovery of strong magnetic fields of lithospheric origin (Acuña et al., 1999, 2001). The Mars Atmosphere and Volatile EvolutioN (MAVEN) spacecraft has collected new magnetic field data in orbit around Mars since November 2014. The primary goal of the MAVEN mission is to analyze Mars's upper atmosphere and ionosphere to quantify processes governing atmospheric loss today and in the past (Jakosky et al., 2015). However, MAVEN magnetometer data can also be used to refine our knowledge of Mars's magnetic field.

Generally, magnetic measurements contain variable contributions from fields of external and internal origin and separation of these is challenging. To address this issue, magnetic proxies can be defined that characterize the strength of external field contributions at a given time. On Earth, different proxies, typically referred to as indices, have been developed using ground-based magnetometers to assess magnetic activity and the strength of different magnetic sources such as the ring current or the auroral electrojets (Kauristie et al., 2017;

Table 1
MAVEN and MGS Orbit Specifications

Orbit characteristics	MGS MO	MGS AB/SPO	MAVEN
Orbit	Nearly circular	Eccentric	Eccentric precessing in latitude and local time
Altitude	370–438 km	Periapses 100–120 km / 170–200 km	150–6,200 km with deep dips to 110 km
Inclination	87°	varying	75°
Local times	2 a.m./2 p.m.	Variable but mostly daytime at altitudes less than MO	Variable local times

Note. AB, SPO, and MO denote the Aerobraking, Science Phasing Orbit and Mapping Orbit mission phases of MGS. MGS = Mars Global Surveyor; MAVEN = Mars Atmosphere and Volatile EvolutioN.

Love & Remick, 2007). These indices have proven useful for modeling of core and lithospheric fields and studies of interior electrical conductivity (Finlay et al., 2017; Kauristie et al., 2017). In November 2018, the InSight mission (Banerdt et al., 2017) will deploy the first ground-based magnetic observatory on Mars. Primary mission goals include an improved understanding of the planet's interior, and surface magnetic field measurements will contribute to this goal.

Proxies for external magnetic fields at Mars could also be very useful. One example for the need of a proxy at Mars is the selection of quiet time magnetic field data for modeling of the lithospheric magnetic field. The lithospheric field has been studied primarily using MGS data (e.g., Arkani-Hamed, 2001; Cain, 2003; Langlais et al., 2004; Morschhauser et al., 2014; Purucker et al., 2000) obtained while the spacecraft was in a highly eccentric orbit during the early Aerobraking, Science Phasing Orbit phases and in the nearly circular Mapping Orbit (MO) phase (Table 1). Different strategies were established to reduce contamination of crustal field models by external fields. Because MGS spent ~7 yrs in a ~400 km altitude orbit, multiple measurements over any given region allowed the selection of only night-side data (defined as in the shadow of the planet) for lithospheric field modeling. Night-side data are less affected by the draped interplanetary magnetic field (IMF) and ionospheric currents than day-side data and are thus typically quieter. However, Ferguson et al. (2005) show that even for night-side measurements the external field is a considerable contribution and care has to be taken to separate this from the crustal field. Furthermore, repeat measurements by MGS have allowed identification and removal of outliers from binned data (e.g., Langlais et al. 2004). Lower altitude measurements collected during early mission phases covered only ~ 20% of the planetary surface (Acuña et al., 1999), and were typically obtained during the day. However, because low-altitude observations capture shorter wavelength features in the lithospheric field, most day-side data from the Aerobraking, Science Phasing Orbit (AB/SPO) phases have been retained in field modeling efforts to date. Possible outliers have been identified via differences between the data and predictions of an initial, previously published model (Lillis et al., 2008) or have been downweighted during the inversion (Morschhauser et al., 2014). An alternative approach to identifying external field activity uses an extrapolation of the Advanced Composition Explorer IMF measurements at the Earth-Sun L1 Lagrange point to Mars (Langlais et al., 2017). This approach, however, is only applicable where Mars is in, or close to, the same Parker Spiral Arm as the Earth (~ 25% of the time).

MAVEN's orbit geometry is quite different from that of MGS during the MO phase. It is much more eccentric with a periapsis that precesses in the body-fixed and local time (Mars Solar Orbit, MSO) frame. This has yielded a substantial increase in the quantity of low-altitude magnetic field measurements that could be used to generate lithospheric field models with correspondingly higher spatial resolution. The nighttime coverage of MGS and MAVEN data, binned in latitude and altitude bins (Figure 1) highlights the different orbit geometries of the two satellites (Table 1). MGS MO data show the many days of repeat measurements (referred to as sampling days in Figure 1) at altitudes around 400 km, whereas lower altitudes are mostly sampled by MAVEN, but often only on a few sampling days. This is important because every time the satellite crosses a given location, the lithospheric field and the time-varying external field are measured. Thus, multiple measurements at the same location enable separation of steady fields of lithospheric origin from time-varying external fields. If there are only a few measurements over a given location at similar altitudes, external fields are harder to identify and can contribute bias to lithospheric field models. However, MAVEN periapsis altitudes on the nightside are typically ~140 km and are as low as ~110 km during Deep Dip campaigns (Zurek et al., 2017). When periapsis is on the nightside, part of the orbit near apoapsis is in the upstream, undisturbed solar wind, and IMF. This provides direct constraints on solar wind conditions and allows us to investigate possible correlations between IMF conditions measured by MAVEN and signals measured at lower

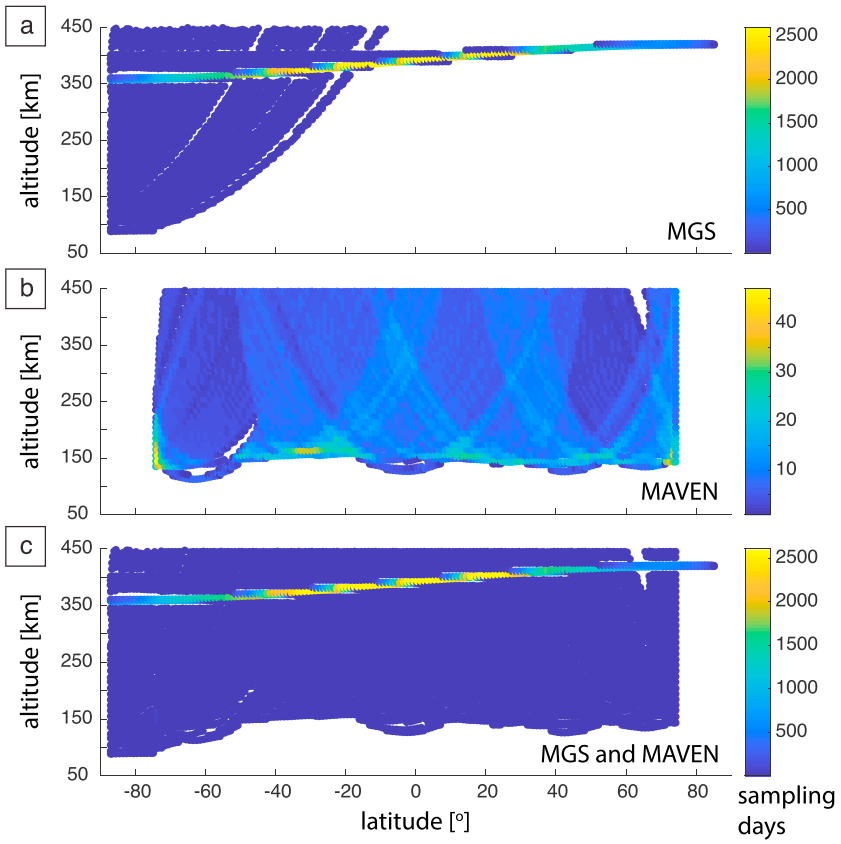

Figure 1. (a) MGS, (b) MAVEN, and (c) MGS and MAVEN combined data distributions, binned in 0.5° longitude × 10 km altitude bins for nightside data. MAVEN data (1 Hz) cover the period November 2014 to November 2017. MGS contains all nighttime data for AB/SPO phases and a reduced data set for the MO phase (every 15 s). Note the different scales for the color bars that show the number of days sampled in each bin. MGS = Mars Global Surveyor; MAVEN = Mars Atmosphere and Volatile EvolutioN.

nightside altitudes on the same orbit well inside the bow shock. Although there is a time delay of up to 2 hr between those measurements, coherence over time intervals of 20 hr was shown for IMF strength, which suggests approximately steady solar wind conditions over the time scale of a MAVEN orbit (Marquette et al., 2018).

Here we propose a magnetic activity proxy that is based on MAVEN magnetic field observations, which could be extended and refined with surface measurements returned by InSight and used to jointly analyze MAVEN and InSight data. We use MAVEN orbits that sample the solar wind near apoapsis to investigate whether IMF conditions measured by MAVEN correlate with signals observed on the same orbit closer to the planet, inside the bow shock (section 2). More generally, we show that the proxy can be extended to orbits for which measurements are not available in the IMF. This may be particularly useful when the MAVEN orbit geometry is changed to be less eccentric as expected for Spring 2019 (R. Lillis, personal communication, 2018), such that the orbit samples the upstream solar wind significantly less frequently. Based on our results, we propose a proxy for solar wind conditions that allows separation of magnetically quiet and noisy orbits (section 3). We demonstrate the utility of the proxy, via a regional crustal field inversion around the future InSight Landing Site (4°N, 134°E), investigating both quiet and noisy data over the region (section 4). Finally, we discuss other applications for the proxy (section 5).

2. Correlation of the IMF and Fields Close to the Planetary Surface

The absence of a strong global magnetic field on Mars means that the solar wind and IMF can interact directly with the ionosphere (e.g., Brain et al., 2003; Halekas et al., 2017; Liu et al., 1999). We suggest that the magnetic field upstream of the bow shock might provide diagnostics for nightside ionospheric and magnetospheric field fluctuations. To study such effects, we make use of the MAVEN orbit configuration and select orbits for

which apoapsis occurred in the solar wind. The shock location is highly dynamic, so rather than identify this on an orbit-by-orbit basis, we defined an outer limit for the shock location as 0.3 martian radii beyond the model shock of Vignes et al. (2000). We retained only orbits on which the start and end points of a 30-min window, centered on the apoapsis time, occurred beyond this outer shock limit, so that the IMF measurements were minimally affected by backscattering and turbulence from the shocked solar wind. We visually checked several orbits to confirm that this choice was sufficiently conservative and also examined our resulting IMF estimates for any anomalous values. We calculated a suite of parameters characterizing the variability and magnitude of the different components of the IMF (in Mars-solar-orbital coordinates) in the 30-min window for each orbit: specifically, the mean, the standard deviation, and the peak-to-peak range.

To estimate external fields close to the planet, we subtracted the crustal field predicted by the model of Morschhauser et al. (2014), hereinafter referred to as M14, from the observed fields at altitudes less than 600 km on the nightside. This leaves what we refer to as the *residual field* and removes large-scale high-amplitude lithospheric fields that have already been well characterized with MGS data. We computed the same statistics for the residual field as for the IMF, except evaluated for field components in spherical polar coordinates in the Mars body-fixed (MBF) frame. Although we do not expect a one-to-one correlation between the IMF components in the MSO frame and crustal field components in the MBF frame, previous work has shown that the horizontal components of the crustal field in the MBF frame are often more contaminated by external fields than the radial component (Cain, 2003). Thus, we analyze the IMF and the crustal field in the frame appropriate to each field. We examined correlation coefficients between IMF and residual field parameters measured from data on the same orbit (Figure 2). The residual field was characterized in two altitude ranges: 300–600 km and below 300 km. We find that several parameters for the IMF and residuals correlate significantly (i.e., the p values are less than 0.05 in Figures 2a and 2b, where p value is the probability of getting a correlation as large as the observed correlation coefficient by random chance, when the true correlation is zero). In particular, at altitudes 300–600 km, the mean residual fields correlate with the mean, variability and peak-to-peak range of the IMF. Weaker correlations are seen at lower altitudes, but notably, there is still a correlation between the mean horizontal components of the residual field (B_ϕ, B_θ, or $B_h = \sqrt{B_\phi^2 + B_\theta^2}$) and the mean value and variability of the IMF magnitude. In both altitude ranges, the strongest correlations in the residual field are associated with the mean magnitude of the IMF, B_{IMF}. Note that mean values are independent of the coordinate system. The results suggest that external field effects persist to altitudes less than 600 km and even to altitudes less than 300 km. This has also been shown previously to be true at MGS MO altitudes by Ferguson et al. (2005). Furthermore, at 300–600 km altitude crustal field signals are well modeled by current crustal field models. Thus, the residual fields are almost entirely non-lithospheric and the correlation of the mean magnitude of the residual field, B_{res} with B_{IMF}, suggests that it may be possible to use residual fields at these altitudes as a proxy for IMF conditions, if measurements in the IMF are not available.

We next investigated the probability of encountering residual fields of a particular magnitude for a given IMF magnitude measured on the same orbit (Figures 2c and 2d). The average IMF magnitude on all our orbits is 3.8 nT. For $B_{\mathrm{IMF}} = 3.8$ nT, 70% of the residuals at altitudes 300–600 km are below 10 nT, and 50% are below 5 nT. As B_{IMF} increases, B_{res} increases systematically as expected from the correlation matrix, until B_{IMF} is about 7 nT. The low number of data obtained during times of higher B_{IMF} results in noisy probability estimates. Below 300 km, the residuals behave similarly, although the B_{res} signals overall are somewhat increased in amplitude, likely reflecting localized, short-wavelength crustal fields not captured by M14.

3. Defining a Mars Magnetic Activity Proxy

For many applications, such as crustal field modeling (Langlais et al., 2004; Morschhauser et al., 2014) or paleopole estimation from satellite data (e.g., Hood & Zakharian, 2001; Langlais & Purucker, 2007; Milbury et al., 2012; Thomas et al., 2018), a separation of data into magnetically quiet and magnetically noisy conditions is useful. Motivated by the results above, we used the mean value of B_{IMF}, 3.8 nT, as a cutoff value, B_{cut}, and defined orbits with B_{IMF} less or greater than B_{cut} as quiet or noisy, respectively. Residuals for $B_{\mathrm{IMF}} < 3.8$ nT are overall independent of the IMF strength but increase for higher IMF strengths. Furthermore, Marquette et al. (2018) found that the IMF strength was more steady for lower-average values, and thus, upstream measurements adequately characterize the value expected later in the MAVEN's orbit when the spacecraft was on the nightside of the planet. Obviously, other choices for B_{cut} are possible and furthermore a continuous proxy

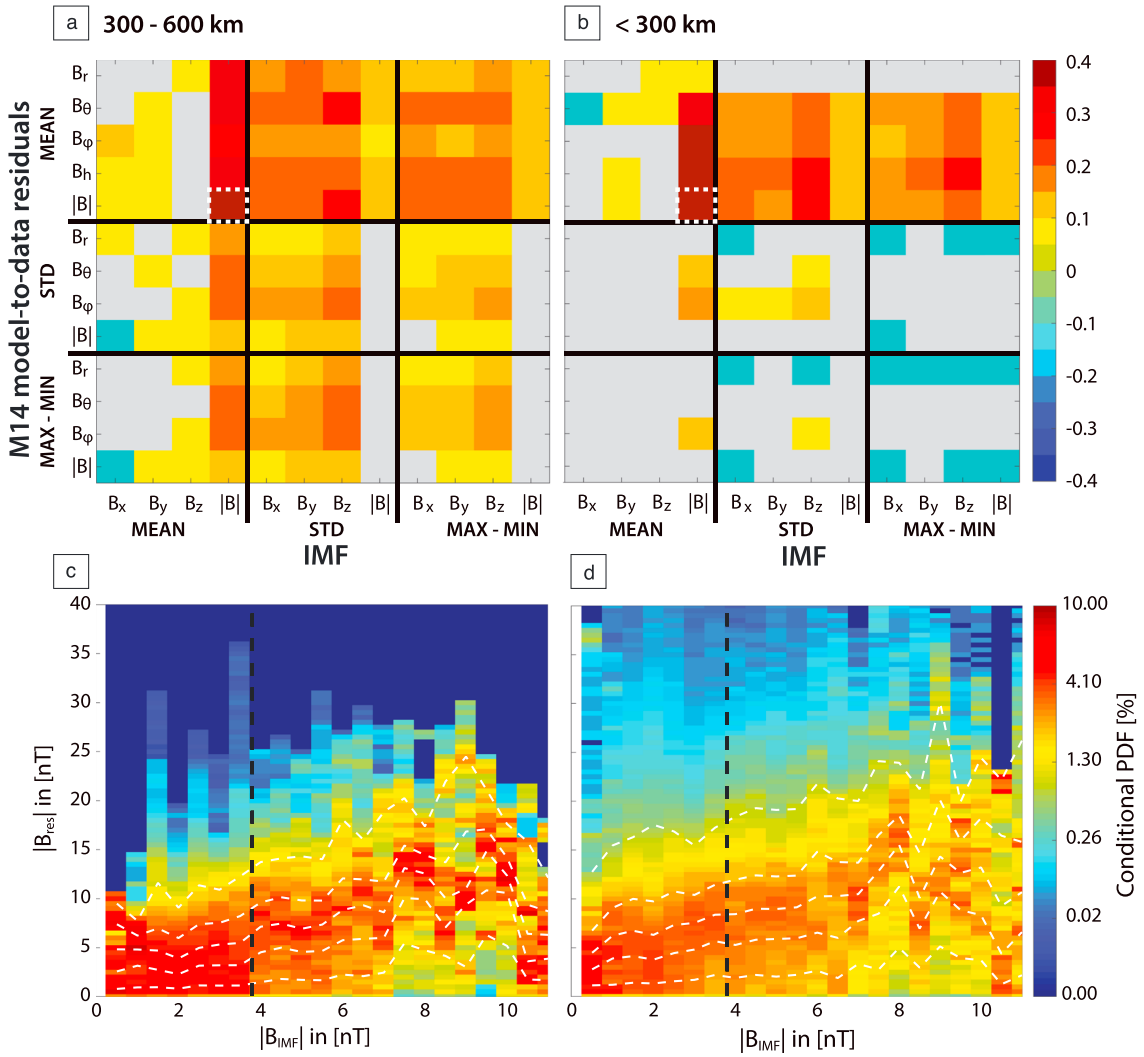

Figure 2. (a, b) Correlation coefficients for various pairs of statistics for the interplanetary magnetic field (IMF) measured in a 30-min window (*x* axis) and residual fields (i.e., data minus the prediction of M14), close to the planet (*y* axis) measured along the same orbit at altitudes of (a) 300–600 km and (b) below 300 km. Gray squares denote correlation coefficients whose values are consistent with no correlation (see section 2). (c, d) Conditional probability density functions showing the probability of an observed residual field magnitude, B_{res}, for a given IMF magnitude, B_{IMF}, corresponding to the element of the correlation matrices outlined by the white dashed boxes, for altitudes (c) 300–600 km and (d) below 300 km. The black dashed lines indicate the mean IMF. The white lines indicate 10th, 30th, 50th, 70th, and 90th percentiles.

could be defined by which orbits are weighted by their relative B_{IMF} values. We chose the simple definition of B_{cut} to demonstrate that this approach can effectively separate quiet and noisy orbits.

This procedure resulted in a quiet data set comprising about 60% of all MAVEN nighttime data below 450 km. A comparison of the altitude dependence of clean and noisy residuals, averaged globally, reveals a clear distinction between the two (Figure 3). We computed the absolute value of the mean of each field component globally in 20-km altitude bins. Consistently lower values are seen for the quiet data, with an ~2 nT offset between the two data sets at altitudes above 300 km. The horizontal components, B_θ and B_φ, show larger average residuals compared with B_r, consistent with larger external field contributions to those components (Brain et al., 2003). At altitudes less than 250 km, we see a steady increase in the average residuals in all components suggestive of crustal field structure not captured by M14. At the lowest altitudes (less than about 150 km) the quiet data proxy is less effective; however, the numbers of data here are smaller and this could also reflect the influence of spatially localized unmodeled crustal fields as well as ionospheric currents.

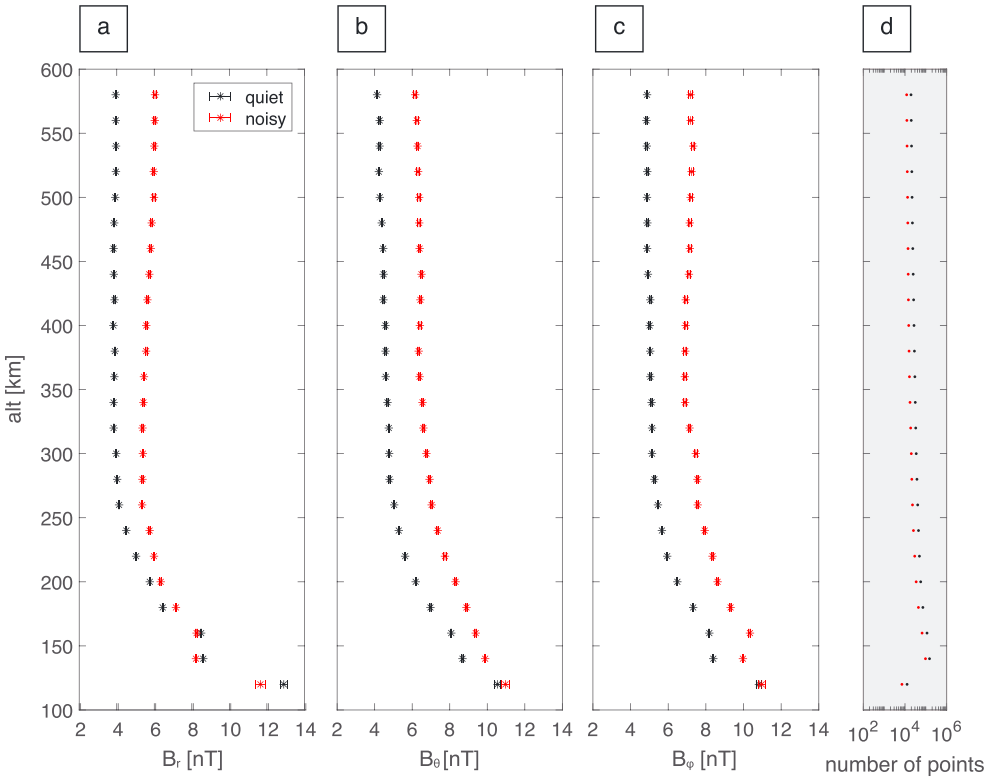

Figure 3. Residual (a) B_r, (b) B_θ, and (c) B_φ fields averaged in 10-km altitude bins for the noisy (red) and quiet (black) data sets and (d) the corresponding number of points in each altitude bin. Horizontal error bars are the standard error in the mean.

4. Application to Local Crustal Field Inversions

Here we demonstrate a use of our proxy by identifying quiet nighttime MAVEN orbits and combining these with nighttime MGS data to invert for crustal magnetization in the vicinity of the InSight landing site (136°E, 4°N). We choose this region as it is not only of interest to the InSight mission and close to the dichotomy boundary, but it is a region of weak crustal fields, where low-altitude MAVEN observations can better constrain the presence or absence of weak magnetization, assuming that quiet data can be suitably identified. For MGS we select nighttime data at MO altitudes, 348–440 km, and average data in each 10-km altitude, 0.5° longitude and 0.5°/sin(θ) latitude bin. In each bin, outliers that were more than 2 standard deviations from the mean were removed and a new average was calculated. This provides a robust average of the field at these altitudes. Nighttime low-altitude (<350 km) measurements for MGS were sparse and none fall in our region of interest. For MAVEN we use vector magnetic field data from November 2014 until August 2017 downsampled to 1 Hz, available from the Planetary Data System, and retain only data below 350-km altitude. These data are not binned because of the strongly varying altitude on any one orbit and the lack of repeat measurements (Figure 1). Application of our proxy results in retention of 65% of the data over our region. We apply an Equivalent Source Dipole method (Mayhew, 1979) using a dipole spacing of 115 km and a mean dipole depth of 20 km. Dipoles within an angular distance of 75° from the observation point contribute to the measurement at each point, following Purucker et al. (1996). The model region encompasses the area of interest: latitude 20°N-20°S, longitude 120–155°E plus an additional 30° in each direction to avoid edge effects. The solution method is a conjugate gradient least squares approach and minimizes the root mean square (rms) difference between data and model predictions. We examined the classic trade-off or *L*-curve (Aster et al., 2011), to select the preferred model. The corner of the *L*-curve was found to be at iteration 11. The resulting dipole moments were converted into an equivalent magnetization assuming a 40-km thick source layer for ease of comparison with previous studies (e.g., Langlais et al., 2004; Voorhies, 2008). The rms misfit of the model to the data is 5 nT; for the MO data alone it is 2 nT, and for data below 200 km altitude it is 6 nT. The overall rms misfit of M14 to the data used in our inversion is 10 nT; for the MO data alone it is only 2 nT, but it is 15 nT for data lower than 200 km. Thus, the new model provides an improved fit to the new low-altitude MAVEN data over the region.

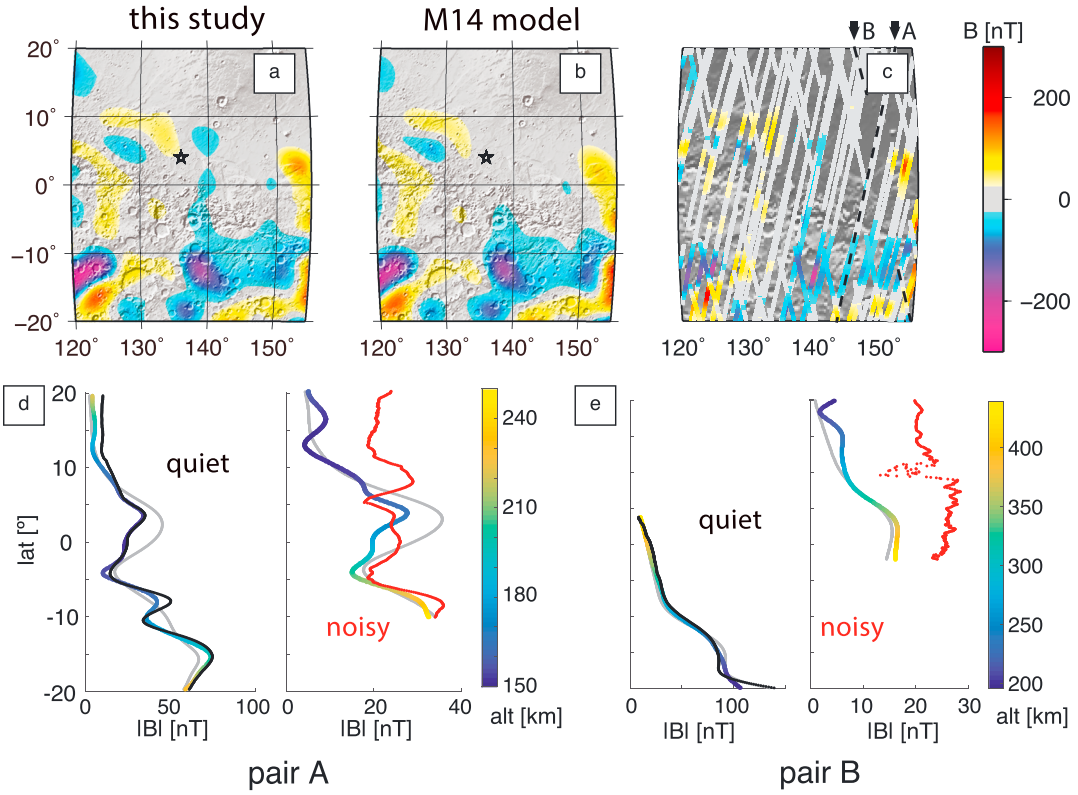

Figure 4. B_r at 150-km altitude in the vicinity of the InSight landing site (black star) predicted (a) by the model derived here and (b) by M14. (c) All nighttime data tracks below 250-km altitude. A and B denote two pairs of orbits with similar tracks; each pair is denoted by a black dashed line (tracks plot on top of one another). (d) Orbit pair A: |B| versus latitude for quiet (black, 2016 day 229) and noisy (red, 2016 day 193) orbits and predicted by M14 (gray) and the model here (color coded by spacecraft altitude). (e) Orbit pair B, figure format as in c (black, 2017 day 37; red, 2016 day 27).

At 150-km altitude our model (Figure 4a) and M14 (Figure 4b) show similar predictions for the magnetic field, with minor differences in amplitude and structure reflecting the only modest additional structure suggested by the low-altitude data (Figure 4c). We computed the rms misfit of our new model to the MAVEN data below 200 km over the region not selected by our quiet proxy and found that this was 50% larger than for the quiet orbits. A model (not shown here) that used all the MAVEN tracks over the region, again chosen from the corner of the L-curve, provided a slightly better fit to the noisy orbits (as expected as these were included in the inversion) but a worse fit to the quiet data and a worse fit overall to the observations below 200-km altitude. We therefore conclude that using the quiet data subset improves our resulting crustal field prediction.

We examined our proxy locally using the predictions from our model along individual tracks. We selected two pairs of orbits (pair A and B in Figure 4c). The ground tracks of each pair are almost the same, but altitudes along each track in the pair are slightly different. Pair A includes one quiet and one noisy orbit (Figure 4d) below 250 km. We observe a good fit of our model to the data for the quiet orbit, but less so for the orbit classified as noisy. M14 shows a comparable fit to the data, but as expected does not capture shorter wavelength information in the MAVEN data. For pair B we chose two orbits covering altitudes up to 450 km, because we expect a good fit of M14 at MO altitudes. The noisy orbit shows higher magnitudes and variability in the magnetic field than the predictions of either M14 or our model.

A comparison of the surface fields predicted by M14 (Figures 5a and 5b) and our model predictions (Figures 5c and 5d) show very similar structure overall, with modest shorter wavelength structure evident in the new inversion. The strongest magnetizations (up to 4.7 A/m for a 40-km thick magnetized layer) are restricted to local regions of the cratered terrain in the south. With the exception of the region around 120°E to 125°E, there is no obvious signature associated with the dichotomy boundary. Magnetization strength in the vicinity of the InSight Landing Site is about 0.3 A/m, suggesting weak (compared to other regions on Mars), but nonzero magnetizations in this region. Also of note is the locally enhanced magnetization at Gale crater (5.4°S, 137.8°E), the exploration target of the NASA Curiosity Rover (e.g., Vaniman et al., 2013).

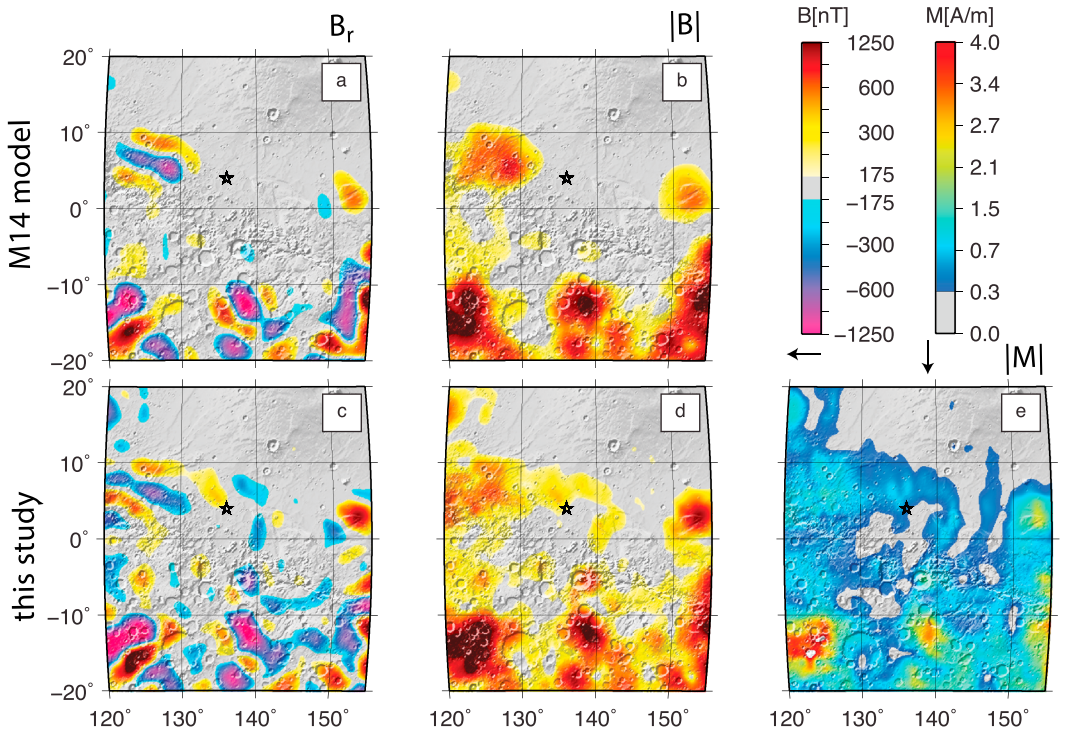

Figure 5. B_r, the radial component (a, c), and the magnitude of the magnetic field (b, d) for the InSight Landing Site are predicted at the planetary surface using this study in (c) and (d) and M14 in (a) and (b). The corresponding model (this study) of the magnetization is shown in (e) where the star indicates the InSight landing Site.

5. Future Applications for the Activity Index

We conclude that the IMF field strength, measured on MAVEN orbits that extend upstream of the bow shock, can be used as a proxy for magnetic field activity on Mars. The resulting identification of quiet or noisy orbits has several applications. First, it is advantageous to the development of high fidelity crustal magnetic field models, especially for data sets like that provided by MAVEN, where multiple repeat measurements over a particular region at the same altitude and local time are not available. Crustal field models of higher spatial resolution than currently available (e.g., Morschhauser et al., 2014) are enabled by low-altitude MAVEN data and are needed to address open questions regarding the magnetization acquisition mechanism, crustal mineralogy, or explanations for the strength of the observed magnetization, and timing of the core dynamo. Second, the InSight Fluxgate Magnetometer (IFG) will provide the first surface measurements of Mars's magnetic field environment. IFG will measure the static crustal and lander fields, as well as time-varying fields from the lander, from external fields, and fields induced in Mars's interior. Magnetic sounding techniques will allow investigations of the electrical conductivity structure of Mars using external time-varying fields and the induced response. The success of these studies, in particular the use the daily and solar rotation periods (Mittelholz et al., 2017), will be greatly aided by identification of data from magnetically quiet times that can be stacked. Conversely, magnetic data from noisy times (e.g., solar events) could be used for elucidating ionospheric inducing fields and electrical conductivity structure at shorter periods. The opportunity of concurrent MAVEN and InSight measurements from orbit and the ground, respectively, will provide the first direct information on external fields at the surface of Mars. Finally, we note that the strong correlation of residual fields, B_{res} with B_{IMF} at 300–600 km altitude suggests that B_{res} at those altitudes might also be used as a proxy for external fields (Figure 2). This may be a useful tool in the event that MAVEN's future orbit geometry does not allow direct measurements of the IMF.

Acknowledgments
We acknowledge support from the University of British Columbia through a Four Year Fellowship (A. M.), the Natural Sciences and Engineering Research Council of Canada, the Canadian Space Agency, and the InSight Mission (C. L. J.). The MGS and MAVEN magnetic field data used in this study are archived in the Planetary Data System, the crustal field spherical harmonic model, M14, is published in the supporting information of Morschhauser et al. (2014). We thank Rob Lillis and an anonymous reviewer for thoughtful comments that improved the manuscript.

References

Acuña, M. H., Connerney, J. E. P., Ness, N. F., Lin, R. P., Mitchell, D., Carlson, C. W., et al. (1999). Global distribution of crustal magnetization discovered by the Mars Global Surveyor MAG/ER experiment. *Science*, *284*(5415), 790–793.

Acuña, M. H., Connerney, J. E. P., Wasilewski, P., Lin, R. P., Mitchell, D., Anderson, K. A., et al. (2001). Magnetic field of Mars: Summary of results from the aerobraking and mapping orbits. *Journal of Geophysical Research*, *106*(E10), 23,403–23,417.

Arkani-Hamed, J. (2001). A 50-degree spherical harmonic model of the magnetic field of Mars. *Journal of Geophysical Research*, *106*(E10), 23197–23208.

Aster, R. C., Borchers, B., & Thurber, C. H. (2011). *Parameter estimation and inverse problems* (2nd ed.). Amsterdam: Elsevier Academic Press.

Banerdt, Boschi, L., Christensen, U., Dehant, V., Giardini, D., Goetz, W., et al. (2013). InSight: A discovery mission to explore the interior of Mars. In *44th Lunar and Planetary Science Conference*, Texas (pp. 1915). https://adsabs.harvard.edu/abs/2013LPI....44.1915B

Brain, D., Bagenal, F., Acuña, M. H., & Connerney, J. (2003). Martian magnetic morphology: Contributions from the solar wind and crust. *Journal of Geophysical Research*, *108*(A12), 1424. https://doi.org/10.1029/2002JA009482

Cain, J. C. (2003). An $n = 90$ internal potential function of the Martian crustal magnetic field. *Journal of Geophysical Research*, *108*, 5008. https://doi.org/10.1029/2000JE001487

Ferguson, B. B., Cain, J. C., Crider, D. H., Brain, D. A., & Harnett, E. M. (2005). External fields on the nightside of Mars at Mars Global Surveyor mapping altitudes. *Geophysical Research Letters*, *32*, L16105. https://doi.org/10.1029/2004GL021964

Finlay, C. C., Lesur, V., Thébault, E., Vervelidou, F., Morschhauser, A., & Shore, R. (2017). Challenges handling magnetospheric and ionospheric signals in internal geomagnetic field modelling. *Space Science Reviews*, *206*(1–4), 157–189. https://doi.org/10.1007/s11214-016-0285-9

Halekas, J. S., Ruhunusiri, S., Harada, Y., Collinson, G., Mitchell, D. L., Mazelle, C., et al. (2017). Structure, dynamics, and seasonal variability of the Mars-solar wind interaction: MAVEN solar wind Ion analyzer in-flight performance and science results. *Journal of Geophysical Research: Space Physics*, *122*, 547–578. https://doi.org/10.1002/2016JA023167

Hood, L. L., & Zakharian, A. (2001). Mapping and modeling of magnetic anomalies in the northern polar region of Mars. *Journal of Geophysical Research: Planets*, *106*(E7), 14,601–14,619.

Jakosky, B. M., Lin, R. P., Grebowsky, J. M., & Luhmann et al., J. G. (2015). The Mars Atmosphere and Volatile Evolution (MAVEN) mission. *Space Science Reviews*, *195*, 3–48. https://doi.org/10.1007/s11214-015-0139-x

Kauristie, K., Morschhauser, A., Olsen, N., Finlay, C. C., Mcpherron, R. L., Gjerloev, J. W., & Opgenoorth, H. J. (2017). On the usage of geomagnetic indices for data selection in internal field modelling. *Space Science Reviews*, *206*, 61–90. https://doi.org/10.1007/s11214-016-0301-0

Langlais, B., Civet, F., & Thébault, E. (2017). In situ and remote characterization of the external field temporal variations at Mars. *Journal of Geophysical Research: Planets*, *122*, 110–123. https://doi.org/10.1002/2016JE005060

Langlais, B., & Purucker, M. (2007). A polar magnetic paleopole associated with Apollinaris Patera, Mars. *Planetary and Space Science*, *55*(3), 270–279.

Langlais, B., Purucker, M., & Mandea, M. (2004). Crustal magnetic field of Mars. *Journal of Geophysical Research*, *109*, E02008. https://doi.org/10.1029/2003JE002048

Lillis, R. J., Frey, H. V., & Manga, M. (2008). Rapid decrease in Martian crustal magnetization in the Noachian era: Implications for the dynamo and climate of early Mars. *Geophysical Research Letters*, *35*, L14203. https://doi.org/10.1029/2008GL034338

Liu, Y., Nagy, A. F., Groth, C. P., DeZeeuw, D. L., Gombosi, T. I., & Powell, K. G. (1999). 3D multi-fluid MHD studies of the solar wind interaction with Mars. *Geophysical Research Letters*, *26*(17), 2689–2692.

Love, J. J., & Remick, K. J. (2007). Magnetic indices. In D. Gubbins & E. Herrero-Bervera (Eds.), *Encyclopedia of geomagnetism and paleomagnetism* (pp. 509–512). Dordrecht, Netherlands: Springer. https://doi.org/10.1007/978-1-4020-4423-6_178

Marquette, M. L., Lillis, R. J., Halekas, J. S., Luhmann, J. G., Gruesbeck, J. R., & Espley, J. R. (2018). Autocorrelation study of solar wind plasma and IMF properties as measured by the MAVEN spacecraft. *Journal of Geophysical Research: Space Physics*, *123*, 2493–2512. https://doi.org/10.1002/2018JA025209

Mayhew, M. A. (1979). Inversion of satellite magnetic anomaly data. *Journal of Geophysics Zeitschrift Geophysik*, *45*, 119–128.

Milbury, C., Schubert, G., Raymond, C. A., Smrekar, S. E., & Langlais, B. (2012). The history of Mars' dynamo as revealed by modeling magnetic anomalies near Tyrrhenus Mons and Syrtis Major. *Journal of Geophysical Research*, *117*, E10007. https://doi.org/10.1029/2012JE004099

Mittelholz, A., Johnson, C. L., & Lillis, R. J. (2017). Global-scale external magnetic fields at Mars measured at satellite altitude. *Journal of Geophysical Research: Planets*, *122*, 1243–1257. https://doi.org/10.1002/2017JE005308

Morschhauser, A., Lesur, V., & Grott, M. (2014). A spherical harmonic model of the lithospheric magnetic field of Mars. *Journal of Geophysical Research: Planets*, *119*, 1162–1188. https://doi.org/10.1002/2013JE004555

Purucker, M., Ravat, D., Frey, H., Voorhies, C., Sabaka, T., & Acuna, M. (2000). An altitude-normalized magnetic map of Mars and its interpretation. *Geophysical Research Letters*, *27*(16), 2449–2452.

Purucker, M. E., Sabaka, T. J., & Langel, R. A. (1996). Conjugate gradient analysis: A new tool for studying satellite magnetic data sets. *Geophysical Research Letters*, *23*(5), 507–510.

Thomas, P., Grott, M., Morschhauser, A., & Vervelidou, F. (2018). Paleopole reconstruction of Martian magnetic field anomalies. *Journal of Geophysical Research: Planets*, *123*, 1140–1155. https://doi.org/10.1002/2017JE005511

Vaniman, D. T., Bish, D. L., Ming, D. W., Bristow, T. F., Morris, R. V., & Blake, D. F. (2013). Mineralogy of a Mudstone at Bay, Yellowknife Crater, Gale. *Science*, *343*, 1–9.

Vignes, D., Mazelle, C., Rme, H., Acuña, M. H., Connerney, J. E. P., Lin, R. P., et al. (2000). The solar wind interaction with Mars: Locations and shapes of the bow shock and the magnetic pile-up boundary from the observations of the MAG/ER Experiment onboard Mars Global Surveyor. *Geophysical Research Letters*, *27*(1), 49–52.

Voorhies, C. V. (2008). Thickness of the magnetic crust of Mars. *Journal of Geophysical Research*, *113*, E04004. https://doi.org/10.1029/2007JE002928

Zurek, R. W., Tolson, R. A., Bougher, S. W., Lugo, R. A., Baird, D. T., Bell, J. M., & Jakosky, B. M. (2017). Mars thermosphere as seen in MAVEN accelerometer data. *Journal of Geophysical Research: Space Physics*, *122*, 3798–3814. https://doi.org/10.1002/2016JA023641